Journal of Molecular Structure 1291 (2023) 135991

Contents lists available at ScienceDirect

Journal of Molecular Structure

journal homepage: www.elsevier.com/locate/molstr

# New azo-azomethine based copper(II) and zinc(II) complexes: Synthesis, electrochemistry, photoluminescence properties, density functional theory calculations and molecular docking

Fatih Purtaş [a], Koray Sayin [b], Gokhan Ceyhan [c], Muhammet Kose [a], Mukerrem Kurtoglu [a,*]

[a] Department of Chemistry, Faculty of Science, Kahramanmaras Sutcu Imam University, Kahramanmaras 46050, Turkey
[b] Department of Chemistry, Faculty of Science, Sivas Cumhuriyet University, Sivas 58140, Turkey
[c] Food Technology Department, Vocational School of Technical Science, Kahramanmaras Sutcu Imam University, 46100 Kahramanmaras, Turkey

ARTICLE INFO

*Keywords:*
Azo-azomethine
Metal chelate
Crystal structure
Fluorescence
Electrochemistry
M062X

ABSTRACT

A new bidentate azo-azomethine ligand 2-{(*E*)-[(3,4-*dimethylphenyl*) *imino*]methyl}-4-[(*E*)-(4-*ethylphenyl*)*diazenyl*]phenol (**2**) and its copper(II) and zinc(II) complexes (**3**) and (**4**) were synthesized and characterized by elemental analysis, $^{1}H/^{13}C$ NMR (for the ligand **2** and its Zn(II) complex) and IR spectral measurements. The structure of the ligand **2** was also determined by single crystal X-ray diffraction. The structure was solved in monoclinic unit cell and $P2_1/n$ space group with final R value of 0.0586. In the structure of the ligand, the imine (CH═N) bond distance is of 1.276(2) Å which confirms the phenol-imine tautmeric form in the crystalline state. In the structure, molecules are stacked by π-π (edge to edge) interactions. The electrochemical and photoluminescence properties of the synthesized azo-azomethine ligand and its metal complexes were investigated. Also, computational studies of related compounds were performed by using M062X/6-31+G level in vacuum. The potential VEGFR2 inhibitory properties of the synthesized ligand and its possible tautomers was investigated by the docking study. As for the ligand structures, azo-imine form is so reactive against the VEGFR2 protein and its docking score and total interaction energy are better than those of other tautomers.

## 1. Introduction

A Schiff base is a nitrogen analogue of an aldehyde or ketone in which the C═O group is replaced by C═N-R group. It is usually formed by condensation of an aldehyde or ketone with a primary amine. Schiff bases are widely used as analytical reactants since they allow simple and inexpensive determination of several organic and inorganic substances [1]. These compounds have often been used as chelating ligands in the field of coordination chemistry and their metal complexes are of great interest for many years [2].

It is well known that N and O atoms play a key role in the coordination of metals at the active sites of numerous metallobiomolecules [3]. Due to their importance in analytical and bioinorganic chemistry, complexes of tetra-coordinated Schiff bases and transition metals are extensively studied [4]. Zinc is the second most common metallic element in biological systems and the only one known to be essential for functions of enzymes in all six of the fundamental classes [5,6]. Zinc can function as active site of hydrolytic enzymes, where it is ligated by hard donors (N or O). It has long been recognized as an important co-factor in biological molecules, either as a structural template in protein folding or as a Lewis acid catalyst that can readily adopt the coordination numbers 4, 5, or 6 [7–9].

In continuation of our previous studies, we investigated the preparation and characterization of various transition metal complexes of novel azo-azomethine compounds [10–15]. In the present work, we report the syntheses and complex formation of an azomethine ligand containing –N═N– chromophore group which was synthesized by the reaction of 5-[(*E*)-(4-*ethylphenyl*)*diazenyl*]-2-hydroxybenzaldehyde and 3,4-dimethylaniline. The reaction may be represented as shown in Scheme 1. We examined its complexing ability with Cu(II) and Zn(II) salts. Theoretical studies of the possible tautomers, azo-imine form **(I)**, azo-enamine form **(II)**, hydrazone-imine form **(III)** are performed by using restricted B3LYP/LANL2DZ level of theory. Optimized structural parameters, vibration frequencies, frontier molecular orbitals (FMOs), UV spectra and molecular electrostatic potential (MEP) maps of relevant tautomers are investigated by computational chemistry methods.

* Corresponding author.
*E-mail address:* mkurtoglu@ksu.edu.tr (M. Kurtoglu).

https://doi.org/10.1016/j.molstruc.2023.135991
Received 3 January 2023; Received in revised form 8 June 2023; Accepted 9 June 2023
Available online 14 June 2023

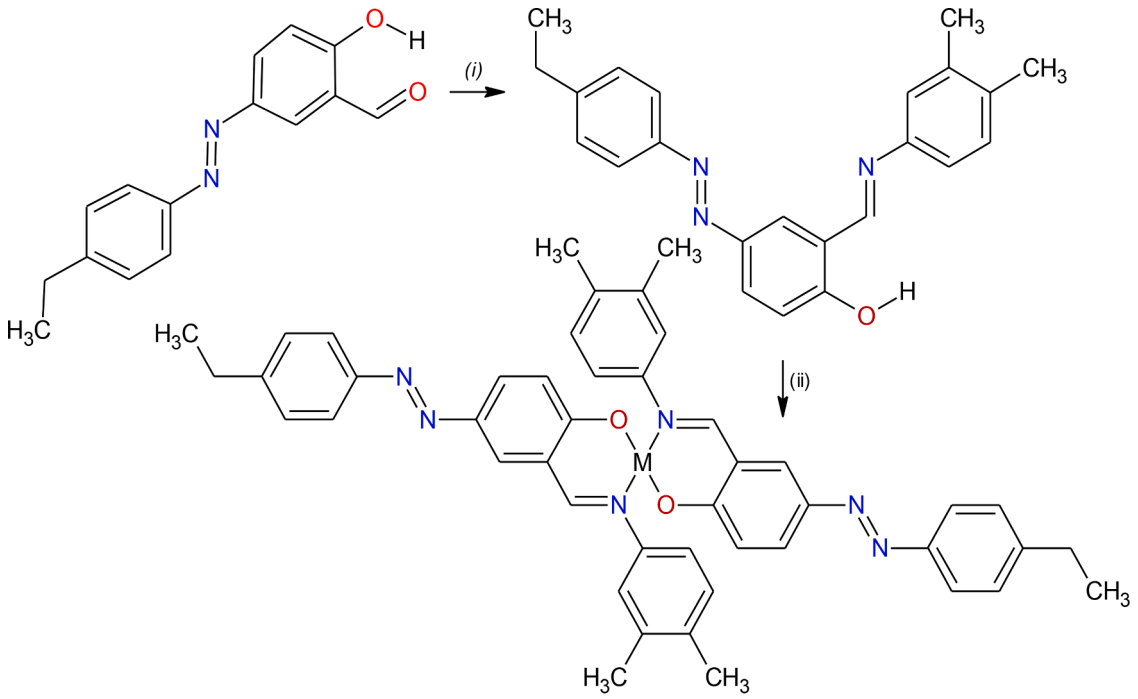


(*i*): 3,4-dimethylaniline, MeOH, reflux; (*ii*): $Cu(CH_3COO)_2.H_2O$ or $Zn(CH_3COO)_2.2H_2O$, $MeOH/CHCl_3$ and reflux.

**Scheme 1.** The synthesis of the azo-azomethine ligand and its metal(II) complexes. (*i*): 3,4-dimethylaniline, MeOH, reflux; (*ii*): $Cu(CH_3COO)_2.H_2O$ or $Zn(CH_3COO)_2{\cdot}2H_2O$, $MeOH/CHCl_3$ and reflux.

Computational chemistry is a significant research area of chemistry for researchers [16–26]. Quantum chemical investigations of related molecules are done by using M062X/6-31+G level in vacuum. Optimized molecule structures, geometric parameters, vibration frequencies, molecular electrostatic potential (MEP) maps, MEP contours, thermodynamic parameters of the bidentate Schiff base ligand containing azo chromophore group and chemical reactivity ranking of related molecules are investigated at M062X/6-31+G level. Biological reactivity of the synthesized azo-azomethine ligand and its metal complexes can be predicted using molecular docking calculations [27–29]. For this aim, biological reactivity of studied compounds is investigated using molecular docking calculations against vascular endothelial growth factor receptor 2 (VEGFR-2). VEGFR2 is important target in anticancer mechanism. Due to the fact that, it is expressed in many cancer types and VEGFR2 promotes cancer cell growth and proliferation [30,31].

## 2. Experimental

### 2.1. Chemicals

All reagents and solvents for synthesis and analysis were purchased from commercial sources and used as received unless otherwise noted. 5-[(*E*)-(4-*ethylphenyl*)*diazenyl*]-2-hydroxybenzaldehyde (**1**) was synthesized according to the standard protocol [32] using 4-ethylaniline and salicylaldehyde (Merck, 99%) as starting materials.

### 2.2. Physical measurements

NMR spectra were performed using a Bruker Advance 400 MHz Spectrometer. The IR spectra were obtained (4000–400 $cm^{-1}$) using a Perkin Elmer spectrum 100 FTIR spectrophotometer. Carbon, hydrogen and nitrogen elemental analyses were performed with a model CE-440 elemental analyser. Single-photon fluorescence spectra of the synthesized ligands and complexes were analysed in the Varian, Cary Eclipse fluorescence spectrophotometer. All samples were analysed by forming solid pellet discs. Data for X-ray crystallography for the ligand **2** were collected at 296(2) K on a Bruker D8 QUEST diffractometer using Mo-Kα radiation (λ = 0.71073 Å). Data reduction was performed using Bruker SAINT [33]. SHELXS97 was used to solved and SHELXL2014/6 to refine the structure [34].

Cyclic voltammograms were made on the Iviumstat Electrochemistry device located in the Chemistry Department, Kahramanmaras Sutcu İmam University, Kahramanmaraş, which has a low current module (BAS PA1) recorder. A galvanic cell was used as an electrochemical cell. A triple electrode system was used in the galvanic cell. Here as the electrode; BAS brand glassy carbon was used as the working electrode (area 4.6 $mm^2$). A platinum wire was used as the counter electrode and a reference electrode filled with $Ag^+$/AgCl with a platinum wire as the auxiliary electrode. Alternate voltammetric measurements were made in a galvanic cell (BAS model C3 cell stand) at room temperature by conditioning the platinum counter electrode and Ag+/AgCl reference electrode and (BAS) glassy carbon electrode. All potentials are reported relative to Ag+/AgCl. The prepared solutions were kept in a nitrogen atmosphere for five minutes before the analysis started, and the oxygen removal process was carried out. Digital simulations were performed using DigiSim 3.0 for Windows (BAS, Inc.). Experimental cyclic voltammograms used for the insertion process have been background subtracted and electronically corrected for ohmic drop.

### 2.3. Synthesis of azo-azomethine ligand, hb (2)

A solution of 3,4-dimethylaniline (0.244 g, 2 mmol) in MeOH (30 mL) was slowly added to a solution of 5-[(*E*)-(4-*ethylphenyl*)*diazenyl*]-2-hydroxybenzaldehyde (0.5084 g, 2 mmol) in MeOH (50 mL). The stirred reaction mixture was refluxed for 3 h. After cooling, an orange precipitate was formed which was collected by filtration, then washed with

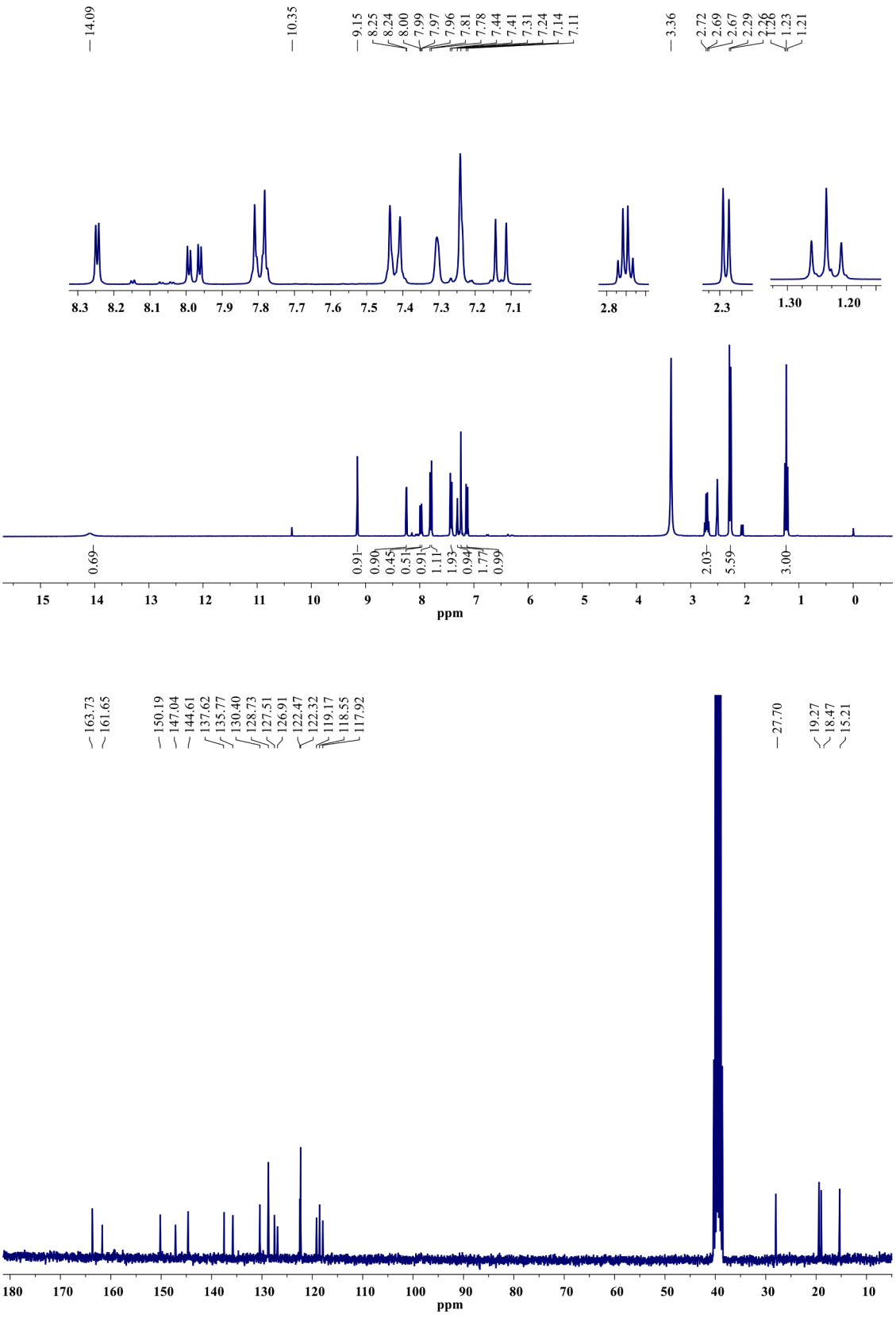


**Fig. 1.** $^{1}H$ (up) and $^{13}C$ (down) NMR spectra of the ligand 2.

cold MeOH, and recrystallized from MeOH.

Yield: 0.4903 g (65%), Color: red crystals. m.p.: 149 °C. *Anal.* Calcld. for $C_{23}H_{23}N_3O$: C, 76.28; H, 6.49; N, 11.76. Found: C, 76.85; H, 6.61; N, 11.56%. $\Lambda_M$: 1.19 $\Omega^{-1}$ $cm^2$ $mol^{-1}$. FT-IR (KBr, $cm^{-1}$): 3434 $\nu$(OH), 2961 $\nu$(Ar-C-H), 2925, 2872 $\nu$(ethyl-C-H), 1619 $\nu$(-C═N-), 1596 $\nu$(-C═C-), 1486 $\nu$(-N═N-). NMR [DMSO-$d_6$, δ(ppm)]; $^1$H: 14.08 (s, 1H, C—OH), 8.25 (s, 1H, CH═N-), 8.24–7.24 (m, 10H, aromatic Hs), 7.143, 7.114 (dd, 2Hd-f aromatic Hs), 3.36 ($CH_2$), 2.71–2.25 (d, 6H, C—$CH_3$ and C—$CH_3$). $^{13}$C: 163.67 (CH═N), 161.70 (Ar-COH), 150.18, 147.16, 144.68, 144.64, 137.50, 135.77, 130.40, 128.73, 127.51, 126.90, 122.46, 122.31, 119.17, 118.55, 117.91 (Ar-Cs), 40.30- 38.63 (solvent Cs), 19.42 and 19.00 ($CH_3$ and $CH_3$), 15.32.

### 2.4. Preparation of copper(II) chelate (3)

The azo-azomethine ligand (0.2 g, 0.558 mmol) was dissolved in $CHCl_3$ (10 mL) and a $Cu(CH_3COO)_2.H_2O$ (0.0555 g, 0.279 mmol) methanolic solution (25 mL) was added with constant stirring over 25 min. The mixture was heated 3–4 h at 50 °C. On cooling crystals were formed. The formed crystals were removed by filtration, washed with water, methanol and finally with ether and dried in a vacuum desiccator.

Yield: 0.2192 g (85%), Color: brown-green powder, m.p.: 248 °C. *Anal.* Calcld. for $C_{46}H_{44}CuN_6O_2$: C, 70.22; H, 6.06; N, 10.56. Found: C, 69.54; H, 5.84; N, 10.58%. IR (KBr, $cm^{-1}$): 3400 s $\nu$(OH), 3021 m $\nu$(Ar-C-H), 2963, $\nu$(ethyl-C-H), 1619 $\nu$(-C═N-), 1598 $\nu$(-C═C-), 1489 m $\nu$(-N═N-), 539 $\nu$(-Cu-O-), 468 $\nu$(-Cu-N-).

### 2.5. Preparation of zinc(II) chelate, (4)

Zn(II) chelate was prepared by the addition of 1 mmol of Zn $(CH_3COO)_2{\cdot}2H_2O$ which was dissolved in about 10 mL of MeOH, into a hot $CHCl_3$ solution of 1 mmol (0.358 g) of the azo-azomethine ligand. The mixture was then refluxed for 3 h. The yellow-orange precipitated solids were filtered off from the cooled reaction mixture. The solid product was washed with cold MeOH and then $Et_2O$, followed by drying at 50 °C overnight.

Yield: 0.4619 g (67%), Color: orange-yellow powder, m.p.: 267 °C. *Anal.* Calcld. for $C_{48}H_{48}ZnN_6O_2$. C, 70.99; H, 5.70; N, 10.80. Found C, 70.87; H, 5.82; N, 10.67%. IR (KBr, $cm^{-1}$): 3500 $\nu$(OH), 2961 $\nu$(Ar-C-H), 2922, $\nu$(ethyl-C-H), 1600 $\nu$(-C═N-), 1588 $\nu$(-C═C-), 1447 $\nu$(-N═N-), 498 $\nu$(Zn-O-), 478 $\nu$(Zn-N). NMR [$CDCl_3$, δ(ppm)]; $^1$H: 8.50, (s, 1H, CH═N-), 8.09–7.24 (10H, aromatic protons), (2H, d aromatic protons), 3.36 ($CH_2$), 2.76–2.68 (d, 6H, $CH_3$), 1.31–1.26 (CH). $^{13}$C: 173.64 (C—O), 168.59, 151.24, 151.09, 146.62, 146.12, 142.99, 138.28, 136.14, 134.73, 130.86, 128.50, 124.60, 122.51, 122.40, 118.40, 117.96, 28.80, 19.85, 19.20, 15.48.

### 2.6. X-ray crystallography

The structure of the bidentate azo-azomethine ligand **2** was solved by direct methods and refined on $F^2$ using all the reflections [34]. All the non-hydrogen atoms were refined using anisotropic atomic displacement parameters and hydrogen atoms bonded to carbon atoms were located at calculated positions using a riding model. In the compound **2**, hydrogen atom bonded phenolic oxygen atom were located from difference maps and refined with temperature factors. Structural details and refinement data are given **Tables S1-S3**.

### 2.7. Computational method

Gaussian software programs [35,36] were used to do computational analyses. At the same time, ChemDraw program was used as a utility for the figure preparation [37]. M062X which is one of the hybrid density functional theory functions was selected as method [38,39] for the computational analysis. As for the basis set, 6-31+G was selected in this study. In complex calculations, LANL2DZ is used as basis set. No imaginary frequency was obtained from calculations.

### 2.8. Molecular docking

Molecular docking analyses of studied compounds were performed at OPLS4 method. For this goal, Maestro 12.2 software were used [36, 40–42]. In these analyses, the target protein was selected as vascular endothelial growth factor receptor 2(VEGFR2) which ID is 3WZE. For the docking calculations some modules which are LigPrep, Protein Preperation, Receptor Grid Generation, Ligand Docking and Ligand Interaction were used.

## 3. Results and discussion

### 3.1. Chemistry

The synthesized metal complexes are coloured solids, and soluble in DMF and DMSO. The lower conductivity values confirmed the non-electrolytic nature of the complexes. The analytical data showed that the metal to ligand ratio is 1:2 of the type $[M(b)_2]$ for Cu(II) and Zn(II) complexes of the azo-azomethine ligand, where **b** stands for deprotonated ligand. The physical and analytical data of the ligand and its metal complexes are depicted in experimental section. No suitable single crystals of the synthesized metal complexes for X-ray studies could be isolated.

### 3.2. Molar conductivity studies

The molar conduction values of synthesized ligand and its metal complexes (2–4) lie within the range of 9–17 $ohm^{-1}cm^2mol^{-1}$, which confirms the non-electrolytic nature of compounds. These findings indicate that the anion is strongly coordinated to the metal center of the complexes.

### 3.3. $^1$H and $^{13}$C NMR spectra

$^1$H and $^{13}$C NMR spectra of the ligand and its Zn(II) complex with the chemical shifts, expressed in ppm downfield from tetramethylsilane, are presented in the experimental section. The chemical shifts of the different types of protons of the investigated azo-azomethine ligand and its Zn(II) complex are also reported. The resonance of protons has been assigned on the basis of their integration and multiplicity pattern. The chemical shifts of the different types of protons found in the $^1$H and $^{13}$C NMR spectra of the ligand is compared with its diamagnetic Zn(II) complex.

The $^1$H and $^{13}$C NMR spectra of the ligand **Hb** in DMSO-$d_6$ are shown in Fig. 1. The $^1$H NMR spectrum of the azo-azomethine ligand showed a signal due to the hydroxyl proton at δ 14.09 ppm. This signal due to OH proton disappeared in the zinc(II) complex in $CDCl_3$, which indicated that there was binding through the oxygen atom of the ligand with deprotonation. A singlet in the spectrum of Hb azo-azomethine ligand at δ 9.15 ppm is assignable to the characteristic peak of the azomethine proton and this signal, in the spectrum of Zn(II) complex, shifted to δ8.50 ppm confirming the coordination of the azomethine nitrogen atom to the Zn(II) center. In the $^1$H NMR spectrum of the ligand **2** and its Zn (II) complex, the signals due to the aromatic protons of the phenyl rings are observed in the δ6.88–8.09 ppm range. The bidentate ligand exhibits a signal for –$CH_2$ protons of the ethyl group at δ2.72 ppm as a quartet. The spectrum of the ligand showed the doublet signals between δ2.26–2.29 ppm region for the protons of the two methyl protons linked aromatic carbons. The signals of the methyl protons of the ethyl group are in the range of ca. δ1.21–1.26 ppm as a triplet.

The $^{13}$C NMR spectrum of the ligand **2** shows 15 sharp peaks corresponding to various aromatic carbon atoms in the suggested molecule expected due to the non-equivalence of the various carbon atoms. In the spectrum of the azo (−N═N−) chromophore group containing azo-

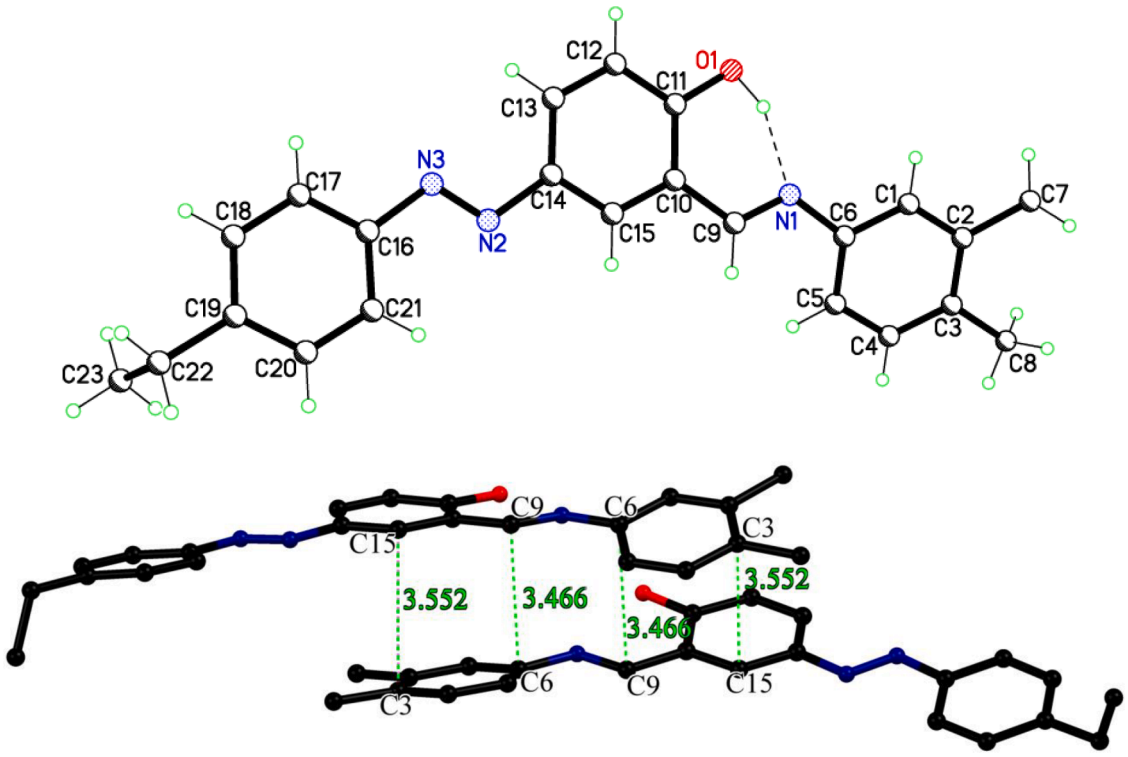


**Fig. 2.** Molecular structure of the ligand 2, with atom numbering. Edge to edge stacking interactions in the structure of the ligand.

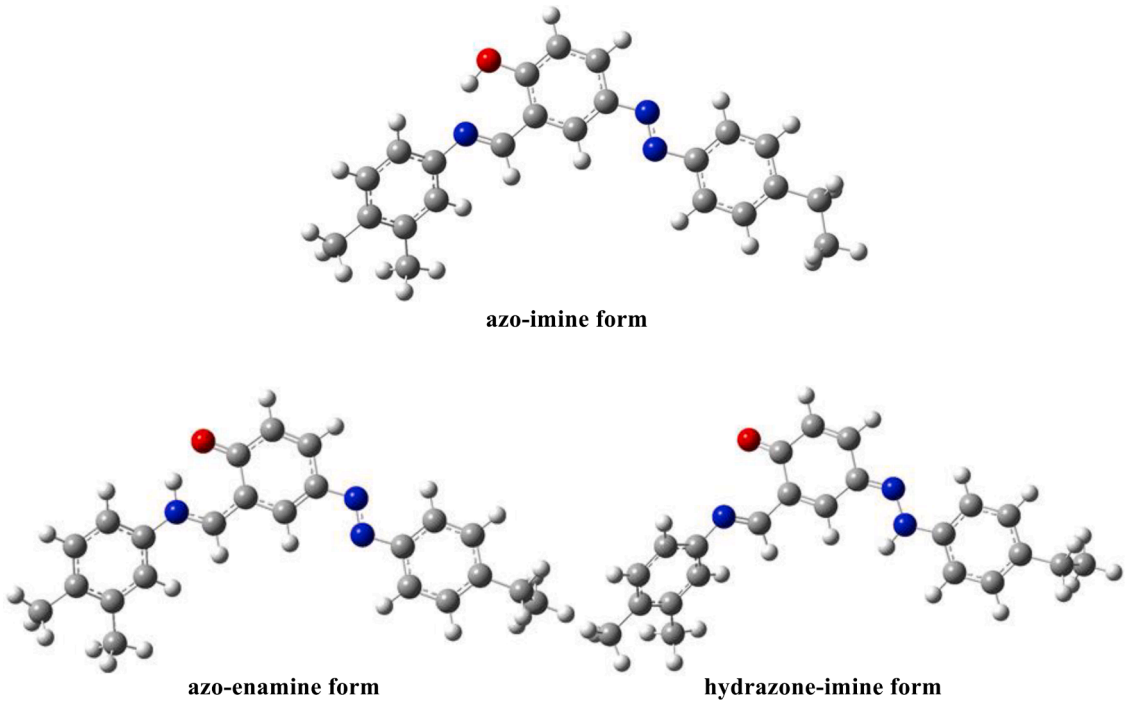


**Fig. 3.** Optimized structure of the related ligand and its tautomers at M06-2X/6-31+G level.

azomethine ligand **2**, the signals at δ163.73 and 161.65 ppm are due to −CH═N− and phenolic C—OH, respectively. The signals appeared in the region of δ150.19–117.92 ppm are assigned to aromatic carbons. In the aliphatic region, there are four signals at δ27.70 ($CH_2$ carbon of ethyl), 19.27 and 18.47 (3,4-$(CH_3)_2$Ar) and 15.21 ($CH_3$ carbon of ethyl) ppm. The results also indicate that the presence of number of carbons agrees well with the expected number of carbons.

In $^{13}C$ NMR spectrum of the Zn(II) complex in $CDCl_3$, the signals due to carbon atom present in the structure were observed. The signals at δ 174.85 and 168.61 ppm were assigned to CH and phenolic CO, respectively. Aromatic carbon signals were observed in the range of δ 119.26–151.10 ppm. In the aliphatic region, there are three signals at δ 56.05 (NC), 28.44 ($CH_2$, ethyl) and 15.90 ($CH_3$, ethyl) ppm. These data are well agreed with proposed structures.

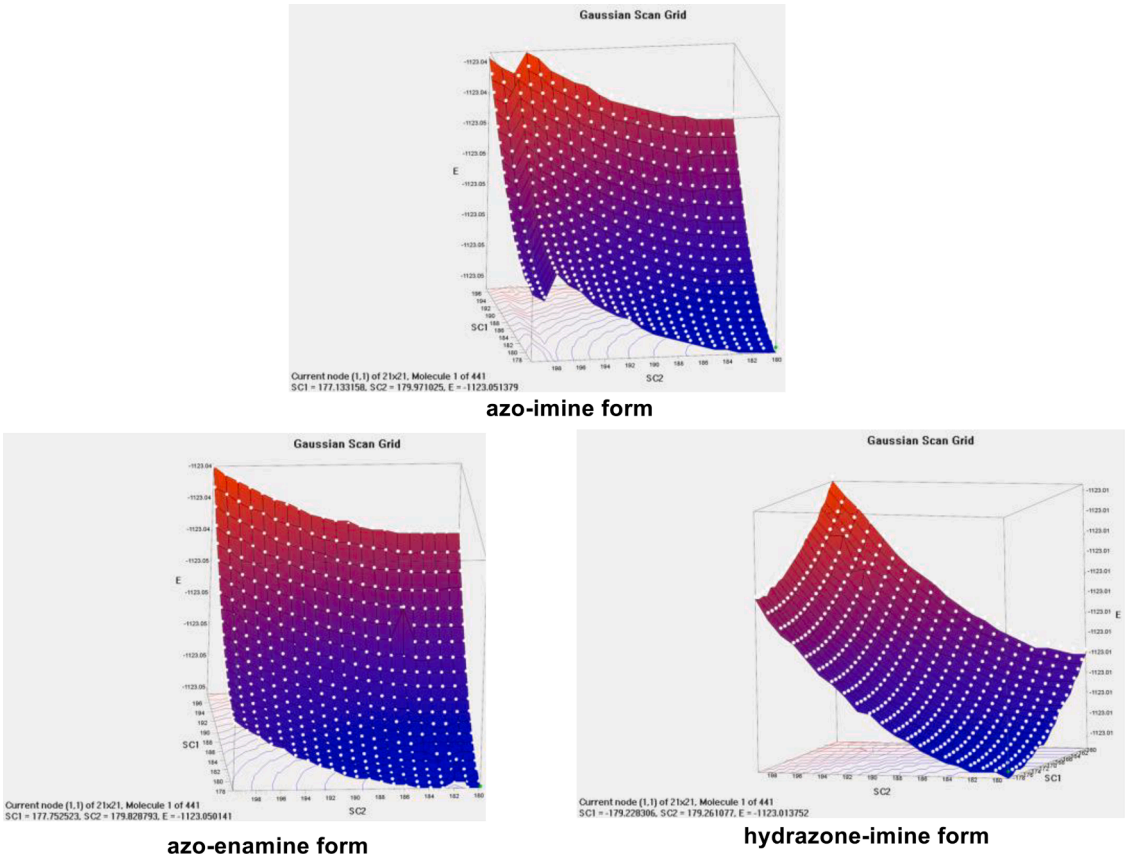


**Fig. 4.** Scan grid of the studied tautomers of the azo-azomethine ligand.

**Table 1**
Thermo-dynamic parameters of related ligand and its tautomers at M062X/6-31+G level in vacuum.

| | $E_{Total}$ (a.u.) | H (a.u.) | G (a.u.) |
|---|---|---|---|
| Azo-imine (I) | −1128.582230 | −1128.581286 | −1128.663977 |
| Azo-enamine (II) | −1128.579953 | −1128.579008 | −1128.661387 |
| Hydrazone-imine (III) | −1128.543651 | −1128.542707 | −1128.626368 |

### 3.4. Infrared spectra

The important infrared frequencies displayed by the bidentate azo-azomethine ligand **2** and its Cu(II) and Zn(II) metal complexes (**3** and **4**) are presented in experimental section. The absorption due to aromatic C—H stretching vibrations was observed in the region 2934–2924 $cm^{-1}$ in all the synthesized compounds.

The characteristic infrared spectral data of the ligand **2** and its Cu(II) and Zn(II) metal complexes are presented in the experimental section. The ligand (**2**) exhibits a medium intense band at 3434 $cm^{-1}$ due to the intramolecular hydrogen bonded (O–H), where its absence in the spectra of Cu(II) and Zn(II) complexes indicates deprotonation of the phenolic group and coordination of the oxygen atom to the metal ion. Infrared spectrum of the ligand shows υ(C═N) peak at 1619 $cm^{-1}$ and absence of C═O peak at around 1650 $cm^{-1}$ in the azo aldehyde indicates Schiff base formation [43]. A downward shift (υ = 4–5 $cm^{-1}$) in υ(C═N) (azomethine) is observed with coordination, indicating that the azo-methine group nitrogen is involved in coordination. It is expected that coordination of nitrogen to the metal atom would reduce the electron density in the azomethine absorption [44]. Some new bands, which are not present in the ligand appeared around 539–498 $cm^{-1}$, corresponding to M-O (478–468 $cm^{-1}$) and M-N vibrations support the involvement of *N* and *O* atoms in coordination with metal center [45]. The above results imply that azo-azomethine ligand **2** coordinates to Cu(II) and Zn (II) metal ions in a bidentate manner with *N,O* donor sites.

### 3.5. X-ray structure of the ligand hb

X-ray quality crystal of azo-azomethine ligand **2** were obtained from slow evaporation of the ligand in methanol solution. Molecular structure of the ligand with atom numbering is shown in Fig. 2. However, the ligand **2** favours phenol-imine tautomeric form although they both have very similar structure. The N1-C9 imine bond distance of 1.276(2) Å is within the range of normal C═N double bond values confirming the phenol-imine form in the solid state. In the structure of the ligand, aromatic rings (C16-C21) and (C10-C15) are in *trans* configuration with respect to the N2-N3 bond. The diazo N2-N3 bond distance is 1.214(2) Å.

The molecule shows intra-molecular hydrogen bonding (O1-H···N1) in the molecule forming a S(6) graph set motif. The outer phenyl rings (C1/C6 and C16/C21) are both twisted from planarity. The dihedral angles between aromatic rings (C1/C6-C10/C15, C10/C15-C16/C21 and C1/C6-C16/C21) are 22.91(6), 7.35(9) and 28.24(7)°, respectively. This may be due to stacking interactions in the structure. The C3-C15 edge of one of the molecules stacks with the same edge of an adjacent molecule (Fig. 2). The C6 and C9 are separated by 3.466 Å. The π-π edge to edge stacking interactions determine the packing of the molecules. The packing diagram of the ligand is given in Fig. S1.

### 3.6. Fully optimization of ligand 2

The synthesized ligand and its possible tautomers are optimized at M06-2X/6-31+G level in gas phase. Optimized structures with atomic labeling are represented in Fig. 3.

Scan analyses are performed and total 441 structures for each form

**Table 2**
Some calculated and experimental structural parameters of M062X/6-31+G level in vacuum.

| Assignments | Experimental | Calculated |
|---|---|---|
| Bond Lengths (Å) | | |
| N1—C9 | 1.276 | 1.294 |
| O1—C11 | 1.345 | 1.357 |
| C14—N2 | 1.458 | 1.424 |
| N3—C16 | 1.449 | 1.427 |
| Bond Angles (deg.) | | |
| C10-C11-O1 | 121.40 | 121.21 |
| C12-C11-O1 | 119.47 | 118.80 |
| C14-N2-N3 | 113.18 | 116.13 |
| N2-N3-C16 | 112.17 | 116.15 |
| O1-H-N1 | 156.00 | 144.61 |
| Hydrogen Bond Lengths (Å) | | |
| O1-H···N1 | 1.730 | 1.697 |

**Table 3**
Some experimental and calculated frequencies ($cm^{-1}$) of mentioned ligand at same level of theory in vacuum.

| | Experimental | Calculated |
|---|---|---|
| $\nu_{OH}$ | 3434 | 2988 |
| $\nu_{CH\text{-}aromatic}$ | 2960 | 3200 |
| $\nu_{CH\text{-}aliphatic}$ | 2960, 2925, 2872 | 3158, 3156, 3059 |
| $\nu_{C=N}$ | 1619 | 1719 |
| $\nu_{C=C\text{-}aromatic}$ | 1596 | 1698 |
| $\nu_{N=N}$ | 1486 | 1590 |

are analysed. Calculated scan grid for studied compounds are represented in Fig. 4.

According to Fig. 4, given structures of the studied tautomers of the ligand have minimum energy and stable ones. Thermo-dynamic parameters of mentioned compounds which are total energy ($E_{Total}$), enthalpy energy (H) and Gibbs free energy (G) are given in Table 1.

According to Table 1, azo-imine tautomer (I) has minimum energy and this result imply that the most stable structure for ligand is azo-imine form. Calculated and experimental structural parameters are given in Table 2.

According to Table 2, there is a well agreement between calculated and experimental structures. Regression coefficient ($R^2$) is calculated as 0.9963. The infrared spectrum of the azo-imine form is calculated at same level of theory and this spectrum is represented in Fig. S2. Some experimental and calculated vibrational frequencies of related ligand are given in Table 3.

Regression coefficient ($R^2$) is calculated as 0.9995 and it implies that there is an agreement between experimental and theoretical results. Mentioned ligand which is azo-imine form is deprotonated and re-optimized at M062X/6-31+G level in vacuum. Optimized structure of deprotonated ligand and molecular electrostatic potential (MEP) map are represented in Fig. 5.

According to Fig. 5, there are red regions at environment of O1 and N1 atoms. This color show that electrons are localized in this region. Mentioned molecule forms a bond with appropriate chemical species by giving electrons from O1 and N1 atoms.

### 3.7. Fully optimization of the Cu(ii) and Zn(ii) complexes

Mentioned complexes are optimized at M062X/LANL2DZ level in vacuum and optimized structures of them are represented in Fig. 6. Additionally, their calculated structural parameters are given in Table 4.

According to Fig. 6 and Table 4, VSPER geometry of Cu(II) and Zn(II) complexes are distorted tetrahedral. Infrared spectra of synthesized complexes are calculated and represented in Fig. S3. The vibrational frequencies of metal complexes are given in Table 5.

### 3.8. Chemical reactivity

Determination of chemical reactivity or reactivity ranking is important for chemical process. In this study, reactivity ranking of related ligand which is azo-imine form and mentioned complexes is determined by using quantum chemical descriptors which are HOMO energy ($E_{HOMO}$), LUMO energy ($E_{LUMO}$), energy gap ($E_{GAP}$), chemical hardness (η), chemical softness (σ), absolute electronegativity (χ), electrophilicity index (ω), nucleophilicity index (N) and dipole moment (μ). Mentioned descriptors are calculated and given in Table 6.

$E_{HOMO}$ is generally related to electron-donating ability and a higher value of $E_{HOMO}$ indicates the tendencies of electron transfer to an appropriate molecule that has a low empty molecular orbital. In respect to HOMO energy, the activity ranking of mentioned molecules should be as follow:

$$3 > 4 > \text{Ligand 2 (azo} - \text{imine form)}$$

$E_{LUMO}$ is other quantum chemical descriptor and mainly associated with electron accepting ability. Low value of $E_{LUMO}$ indicates the tendencies of electron transfer from appropriate molecule to studied molecule. If $E_{LUMO}$ is decisive in determining the chemical reactivity ranking, the activity ranking of mentioned molecules should be as follow:

$$\text{Ligand 2 (azo} - \text{imine form)} > 3 > 4$$

Another essential parameter is the energy gap ($E_{GAP}$) between HOMO and LUMO. The smaller GAP energy shows the more reactive. The chemical hardness and softness are other essential parameters. The chemical reactivity tendencies of compounds towards appropriate molecules can be discussed with HSAB (hard-soft-acid-base) approximation. The reactivity is increased with the increasing of softness value and decreasing of hardness value. According to the $E_{GAP}$ and softness values, the ranking of biological reactivity should be as follow.

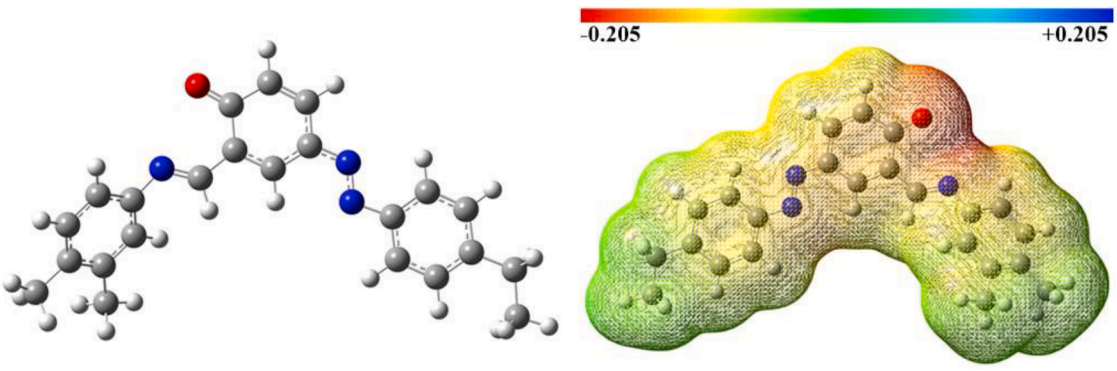


**Fig. 5.** Optimized structure and MEP map of related molecule at M062X/6-31+G level in vacuum.

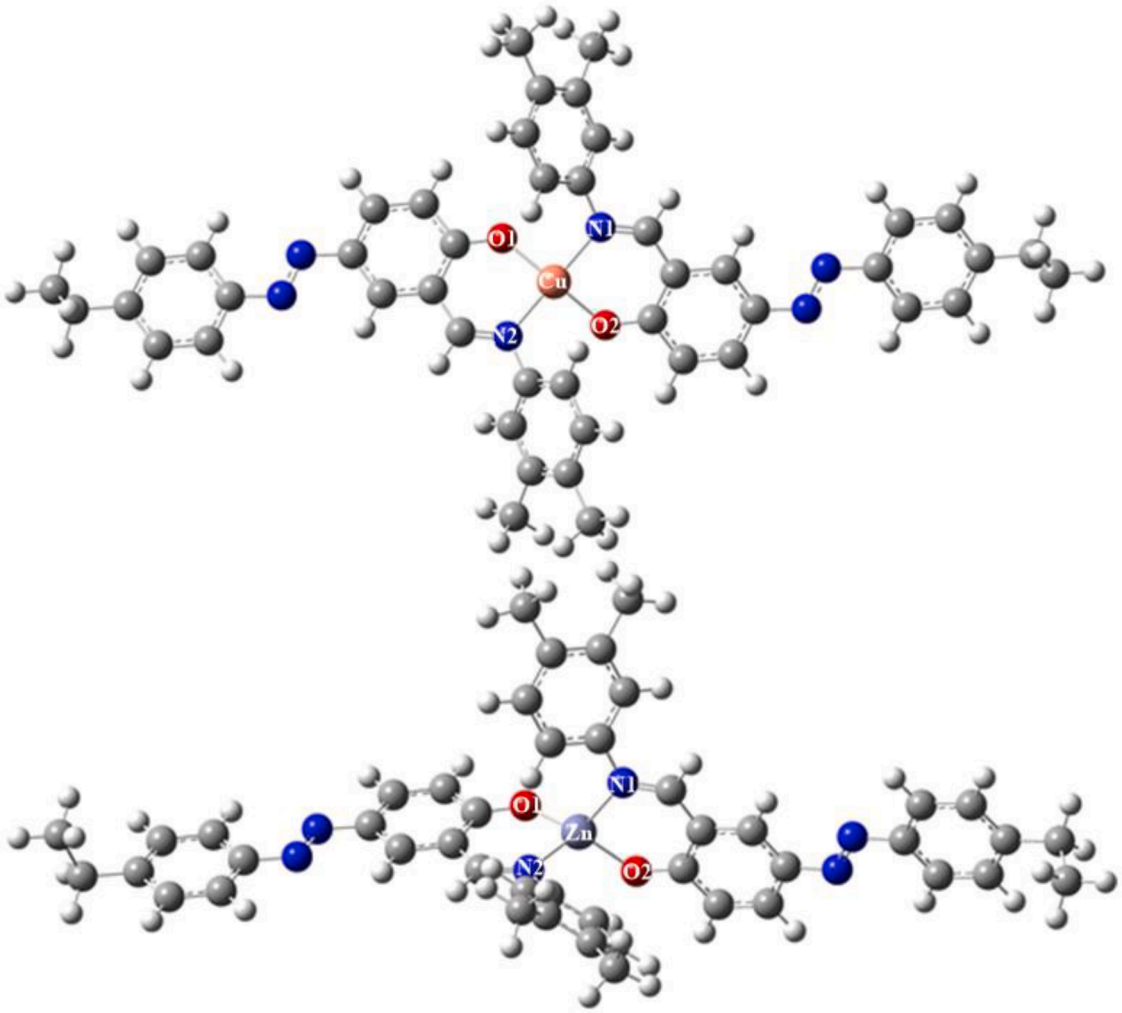


**Fig. 6.** Optimized structures of Cu(II) and Zn(II) complexes at M062X/LANL2DZ in vacuum.

**Table 4**
Some calculated and experimental structural parameters of M062X/6-31+G level in vacuum.

| | Cu complex | Zn complex |
|---|---|---|
| Bond Lengths (Å) | | |
| M—N1 | 2.021 | 2.075 |
| M—N2 | 2.021 | 2.082 |
| M—O1 | 1.903 | 1.933 |
| M—O2 | 1.903 | 1.940 |
| Bond Angles (deg.) | | |
| N1-M-O1 | 93.17 | 119.13 |
| N1-M-O2 | 155.27 | 111.25 |
| N1-M-N2 | 91.92 | 92.63 |
| O1-M-N2 | 91.95 | 92.12 |
| O1-M-O2 | 155.93 | 128.06 |
| N2-M-O2 | 93.17 | 92.63 |

$4 > 3 >$ Ligand 2 (azo − imine form)

Electronegativity is related with flexibility of electron mobility. The reactivity of molecule increases with decreasing of electronegativity value. In respect to absolute electronegativity, the reactivity ranking should be as follow.

$4 > 3 >$ Ligand 2 (azo − imine form)

Electrophilicity index and nucleophilicity index are other descriptors. Electrophilicity index is associated with electrophilic attack while nucleophilicity index is related to nucleophilic attack. Therefore, reactivity is increased with the increasing of nucleophilicity index and decreasing with electrophilicity index. As a result, the ranking should be as follow:

$4 > 3 >$ Ligand 2 (azo − imine form)

The final descriptor is dipole moment and it has been used in many published papers. Chemical reactivity of compounds increases with increasing of these parameters. According to this explanation, activity ranking should be:

$4 > 3 >$ Ligand 2 (azo − imine form)

**Table 5**
The calculated vibrational frequencies ($cm^{-1}$) of the metal complexes.

| Assignments | Cu Complex | Zn Complex |
|---|---|---|
| $\nu_{CH\text{-}aromatic}$ | 3260–3209 | 3268–3202 |
| $\nu_{CH\text{-}aliphatic}$ | 3175–3058 | 3172–3058 |
| $\nu_{C=N}$ | 1705 | 1705 |
| $\nu_{C=C}$, $\nu_{C=N}$, $\nu_{C=O}$ | 1690 | 1688 |
| $\nu_{C-N}$ | 1675 | |
| $\nu_{C-C}$ | 1612 | 1611 |
| $\nu_{N-N}$ | 1555 | 1553 |
| $\nu_{C=O}$ | 1525 | 1525 |
| $\nu_{M\text{-}O}$, $\nu_{M\text{-}N}$ | 514 | 513 |

**Table 6**
Calculated quantum chemical descriptors for ligand and its complexes.

| Compounds | $E_{HOMO}$[a] | $E_{LUMO}$[a] | $E_{GAP}$[a] | $\eta$[a] | $\sigma$[b] | $\chi$[a] | $\omega$[a] | N[b] | $\mu$[c] |
|---|---|---|---|---|---|---|---|---|---|
| azo-imine (I) | −7.129 | −1.397 | 5.733 | 2.866 | 0.349 | 4.263 | 3.170 | 0.315 | 4.208 |
| 3 | −6.793 | −1.311 | 5.481 | 2.741 | 0.365 | 4.052 | 2.995 | 0.334 | 2.163 |
| 4 | −6.676 | −1.381 | 5.295 | 2.648 | 0.378 | 4.029 | 3.065 | 0.326 | 7.143 |

[a] in eV.
[b] in $eV^{-1}$.
[c] in Debye.

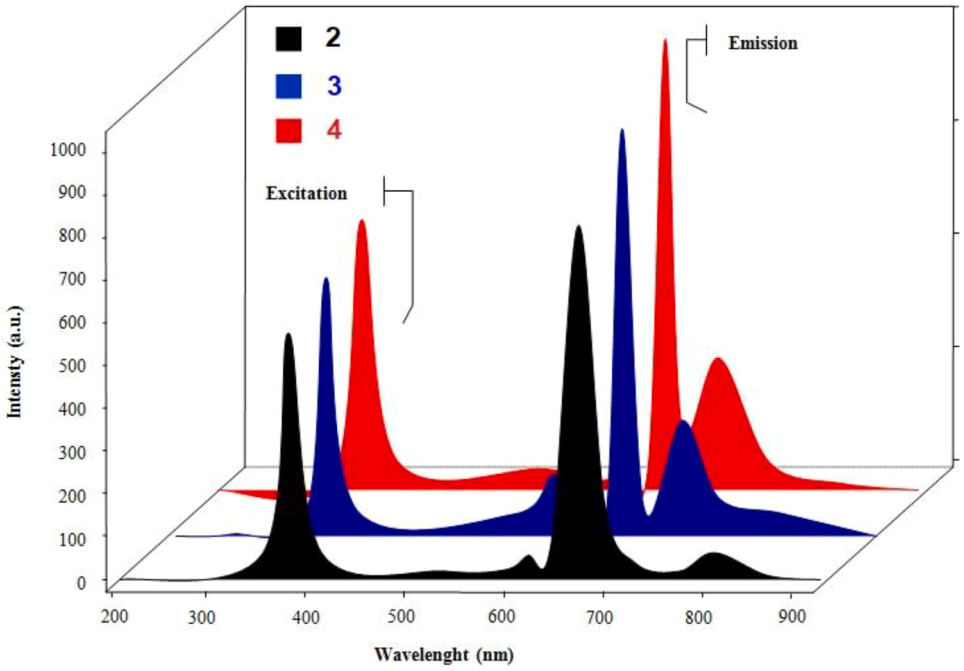


**Fig. 7.** Emission and excitation spectra of the azo-azomethine ligand (2) and its metal complexes (3 and 4).

**Table 7**
Photoluminescence and absorption data of the synthesized ligand and its metal complexes.

| Compound | $\lambda_{max}$ | | |
|---|---|---|---|
| | Exc. (Intensity) | Em. (Intensity) | Abs. (nm) |
| **2** | 391 (530) | 635 (36), 669 (805), 816 (42) | 336 |
| **3** | 395 (538) | 642 (214), 671 (985), 756 (324) | 274, 370 |
| **4** | 393 (542) | 592 (76), 680 (831), 761 (403) | 301, 380 |

As a result, zinc(II) complex has higher activity than the free ligand and its Cu(II) complex.

### 3.9. Absorption and photoluminescence spectral studies

The electronic properties of the azo-azomethine ligand and its Cu(II) and Zn(II) complexes were investigated in DMF solvent ($1 \times 10^{-4}$ M). Photoluminescence excitation spectra were measured at 230 V using a 1000 W xenon flash lamb combined with a grating Monk-Gilleson type monochromator (50 or 60 Hz) using low stray light as an excitation source. The photoluminescence signal passed through a grille monochromator with a central distance of 500 mm and passed through a bright 500 gauge / mm grid at 1200 nm. The optical signals were then detected with gated photomultiplier with modified S5 response for operation to about 650 nm and strengthened by locking techniques [45].

The photoluminescence properties of azo-azomethine ligand (**2**) and its Cu(II) and Zn(II) complexes (**3** and **4**) were investigated using solid powder technique. For this, a Varian, Cary Eclipse fluorescence spectrophotometer model photoluminescence device was used. First of all, the metal complexes were pelletized by agitating the agate well and pressing in the solid apparatus part. The slit settings are set to ±5. First a pre-scan was performed to determine the excitation and emission bands. When a pre-scan was first performed on the ligand, an excitation band and an emission band were observed. The emission and excitation spectra of the metal complexes are shown in Fig. 7 and the obtained data are given in Table 7. The synthesized Cu(II) and Zn(II) complexes (**3** and **4**) exhibit one excitation band at 350–420 nm range. This excitation band shifted to higher wavelengths in the spectrum of the Cu(II) complex.

The peak in the excitation spectrum of the Zn(II) complex is stronger than the other peak of the Cu(II) excitation band. Furthermore, the emission spectrum of the Zn(II) complex shows three peaks, one strong peak at 755 nm, seems to Cu(II) metal complex.

In the emission spectra of the synthesized compounds, the copper complex showed three band in the 625, 680 and 810 nm respectively in solid state. On the other side the zinc complex, the band at 600 nm shifted to the longer wave number at 800. The zinc complex indicates three emission bands. In the emission spectra of the ligand, three band at 625, 680, 810 nm was observed in the solid state. But one strong emission band 680 nm. The presence of metal has effect on the excitation spectra of the ligand and its transitional metal complexes. Moreover, phenyl group on the π-bonds have the electron donating property to the aromatic ring by the mesomeric and inductive effects [46].

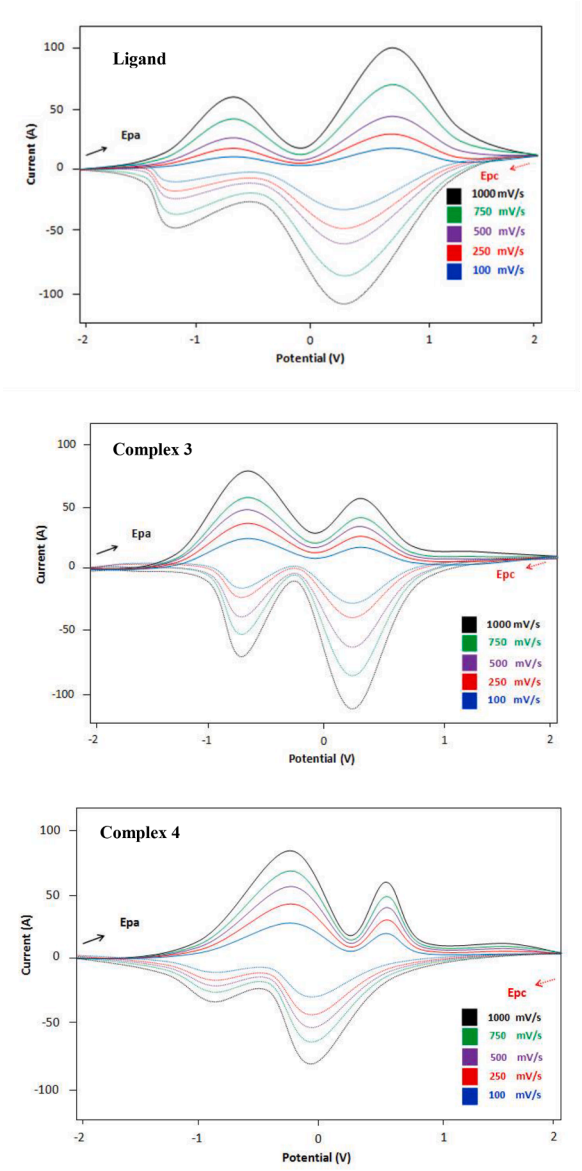


**Fig. 8.** Cyclic voltammograms of the azo-azomethine ligand (2) and its metal complexes (3 and 4) in the presence of 0.1 M $NBu_4BF_4$-DMF solution at different scan rates.

### 3.10. Electrochemistry

Electrochemical properties of the bidentate azo-azomethine ligand and its metal complexes were investigated in DMF-3 M $Bu_4NBF_4$ as supporting electrolyte at 293 K (Fig. 8). All potentials quoted refer to measurements run at scan rates in the 100, 250, 500, 750, 1000 $mVs^{-1}$ and against an internal ferrocene–ferrocenium standard. The electrochemical studies were studied in the $1 \times 10^{-5}$ M DMF solutions and obtained data are given in Table 8.

When the obtained voltammograms are examined; there are two reduction potentials (−0.89, 0.85 V) and two oxidation potentials (0.30–1.30 mV/s) belonging to the ligand. At all scan rates, the ratio of the anodic current to the cathodic current intensity is not one (Ipa / Ipc #1), so it shows irreversible voltammetry.

In DMF ($1 \times 10^{-5}$ M), Cu(II) complex (**3**) shows the reversible redox processes (Ipa: Ipc = 1.0) at all scan rates. The complex has the two anodic peak potentials in the −0.84-(0.34) V range at 100–1000 mV/s scan rates. In addition, the complex has two cathodic peak in the 0.35-(−0.84) V range. The zinc (II) complex (**4**) shows irreversible redox processes in the $1.0 \times 10^{-5}$ M solution at all scan rates. By the increasing of the scan rate, while the cathodic peak potentials shifted to the negative regions, the anodic peaks were shifted to the more positive regions. When the scan rate of the ligand decreases to $1 \times 10^{-5}$ M, the anodic and cathodic peak potential data was both reduced and increased [47].

In cyclic voltammetry, the oxygen atoms on the carbonyl groups of organic compounds resonate to donate electrons to the benzenoid ring and then to the nitrogen atom. The process here is called reversible. Ligand 2 has only one $–CH_2CH_3$ group, while in other complexes (3 and 4) Ligand 2 has two methyl groups (meta and para positions on the benzene ring). Methyl groups decrease the electron density of the benzenoid rings with the inductive effect, while increasing the electron density with the mesomeric effect. The groups that donate electrons to the benzene rings have shifted the potentials from the positive region to the negative region. As a result, the anodic and cathodic data obtained in DMF are shifted to more negative regions in the complexes. The potentials for reduction or oxidation of transitional metal complexes containing highly electron-withdrawing groups at the methyl positions of

**Table 8**
The electrochemical date of the ligand (**2**) and its metal complexes (**3** and **4**).

| Compound | Scan-rate (mV/s) | $E_{pa}$(V) | $E_{pc}$(V) | $I_{pa}/I_{pc}$ | $E_{1/2}$(V) | $\Delta E_p$(V) |
|---|---|---|---|---|---|---|
| **2** | 100 | −0.85, 0.85 | 0.26, −1.26 | 0.67 | – | 0.59 |
| | 250 | −0.86, 0.84 | 0.27, −1.27 | 0.66 | – | 0.59 |
| | 500 | −0.87, 0.83 | 0.28, −1.28 | 0.65 | – | 0.59 |
| | 750 | −0.88, 0.82 | 0.29, −1.29 | 0.64 | – | 0.59 |
| | 1000 | −0.89, 0.81 | 0.30, −1.30 | 0.63 | – | 0.59 |
| **3** | 100 | −0.80, 0.30 | 0.31, −0.80 | 1.00* | | 0.90 |
| | 250 | −0.81, 0.31 | 0.32, −0.81 | 1.00* | | 0.92 |
| | 500 | −0.82, 0.32 | 0.33, −0.82 | 1.00* | | 0.94 |
| | 750 | −0.83, 0.33 | 0.34, −0.83 | 1.00* | | 0.96 |
| | 1000 | −0.84, 0.34 | 0.35, −0.84 | 1.00* | | 0.98 |
| **4** | 100 | −0.40, 0.51 | −0.10, −0.93 | 0.43 | – | 0.61 |
| | 250 | −0.41, 0.52 | −0.11, −0.94 | 0.43 | – | 0.63 |
| | 500 | −0.42, 0.53 | −0.12, −0.95 | 0.44 | – | 0.65 |
| | 750 | −0.43, 0.54 | −0.13, −0.96 | 0.44 | – | 0.67 |
| | 1000 | −0.44, 0.55 | −0.14, −0.97 | 0.45 | – | 0.69 |

All the potentials are referenced to $Ag^+$/AgCl; where $E_{pa}$ and $E_{pc}$ are anodic and cathodic potentials, respectively. $\Delta E_p = E_{pa} – E_{pc}$. $E_{1/2} = 0.5$ x ($E_{pa} + E_{pc}$). (Ipa/Ipc = 1, Reversible).

**Table 9**
Molecular docking results of the possible tautomers of the ligand (2) and its metal complexes (3 and 4).

| Compounds | DS[a] | $E_{vdW}$[a] | $E_{Coul}$[a] | $E_{Total}$[a] |
|---|---|---|---|---|
| azo-imine (I) | −9.092 | −45.560 | −6.228 | −51.788 |
| azo-enamine (II) | −7.576 | −49.774 | −0.053 | −49.827 |
| hydrazone-imine (III) | −6.336 | −47.256 | 0.509 | −46.748 |
| 3[b] | ND | ND | ND | ND |
| 4[b] | ND | ND | ND | ND |

[a] in kcal/mol.
[b] ND: No Docked.

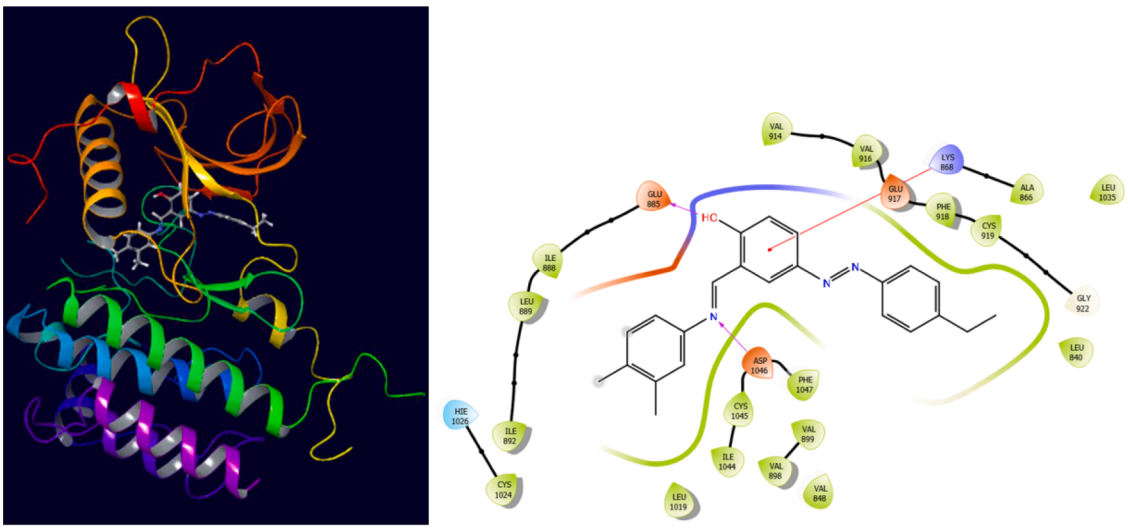


**Fig. 9.** The docking structure and interaction map of azo-imine tautomer with 3WZE.

the unconsolidated electron pair on oxygen will depend upon the electronic properties of the azo group. When we look at the voltammograms, we see that the strongest peak is derived from the potential of reduction.

### 3.11. *Molecular docking*

The biological activity can be investigated experimentally and computationally. Especially, quantum chemical parameters, QSAR studies, molecular docking studies can be used in computational analyses. For this purpose, the better technique is molecular docking analyses due to the fact that receptor – protein interactions can be investigated only molecular docking calculations in computational analyses. In this study, the target protein is selected as 3WZE. Because it is known that the inhibition of VEGFR2 is one of the anticancer mechanisms. The biological activity of studied compounds is investigated against 3WZE, VEGFR2 protein. The x-y-z coordinate of receptor binding domain in 3WZE is 22.88–24.55–36.82, respectively. The docking calculations were performed and the docking score (DS), van der Walls energy ($E_{vdW}$), Coulomb energy ($E_{Coul}$) and total interaction energy ($E_{Total}$) are given in Table 9.

According to Table 9, complex structures are not active against the 3WZE due to the high molecular volume. As for the ligand structures, azo-imine form is so reactive against the VEGFR2 protein. Its docking score and total interaction energy are better than those of others. Docking score implies the harmony between receptor – protein while total interaction energy shows the interaction strength between inhibitor and protein. It can be said that azo-imine form can be considered as inhibitor candidate for the VEGFR2. The docking structure and interaction map of azo form are represented in Fig. 9.

According to Fig. 9, hydrophobic interactions, hydrogen bond, negative and positive charge interactions, solvent exposure and pication interactions are dominant.

## 4. Conclusion

In the present work, we have described the synthesis of bidentate azo-azomethine ligand 2-{(*E*)-[(3,4-*dimethylphenyl*)*imino*]methyl}-4-[(*E*)-(4-*ethylphenyl*)*diazenyl*]phenol (**2**) and its Cu(II) and Zn(II) complexes (**3** and **4**). The molecular structures of the newly synthesized compounds were characterized by various physical and spectroscopic techniques. From elemental analysis and molar conductivity measurements, it is concluded that the metal to ligand ratio is 1:2 stoichiometry of the type $[M(L)_2]$ for Cu(II) and Zn(II) complexes. The definite structure of the ligand was further determined by single crystal XRD study. The compound showed the phenol-imine intramolecular hydrogen bond. The molecule is in phenol-imine tautomeric form in the crystalline state. Crystal structure of the compound was stabilised by π-π interactions. Computational studies of the ligand and its metal complexes were performed by using M062X/6-31+G and M062X/LANL2DZ levels, respectively. Then, ligand is deprotonated and active regions are determined by MEP map. Additionally, chemical reactivity ranking is determined by using quantum chemical descriptors. The biological activity of studied compounds against VEGFR2 is investigated by moleculer docking analyses. In docking results, ligand can inhibit the VEGFR2 while complex structures are inactive against VEGFR2. We investigated photoluminescence and electrochemical properties of the synthesized compounds. The ligand 2 and metal complexes (3 and 4) show the emission bands at the higher wavelenghts.

## CRediT authorship contribution statement

Fatih Purtaş: Synthesis, NMR and mass investigations, Formal analysis, Writing - Original Draft. Koray Sayin: Computational approach, Writing - Original Draft, Writing - Review & Editing. Gokhan Ceyhan: Electrochemistry, photoluminescence analysis, Writing - Original Draft, Writing - Review & Editing. Muhammet Kose: Single crystal structure description, Writing - Original Draft, Writing - Review & Editing. Mukerrem Kurtoglu: Writing - Original Draft, Supervision, Funding acquisition, Project administration.

## Declaration of Competing Interest

The authors declare no conflict of interest.

## Data availability

The authors do not have permission to share data.

## Acknowledgments

This work was supported by the KSU Scientific Research Unity (Project No: 2013/2–33D). The numerical calculations reported in this paper are performed at TUBITAK ULAKBIM, High Performance and Grid Computing Center (TRUBA Resources).

## Supplementary materials

Supplementary material associated with this article can be found, in the online version, at doi:10.1016/j.molstruc.2023.135991.

## References


[1] Z. Cimerman, N. Galic, B. Bosner, The Schiff bases of salicylaldehyde and aminopyridines as highly sensitive analytical reagents, Anal. Chim. Acta 343 (1997) 145–153, https://doi.org/10.1016/S0003-2670(96)00587-9.

[2] P.G. Joshi, P. Phalswal, A. Gaikwad, M.S. More, P.K. Khanna, Schiff base metal complexes driven quantum dots of ZnSe and CdSe, Inorg. Chem. Commun. 135 (2022), https://doi.org/10.1016/j.inoche.2021.109070.

[3] L.A. Saghatforoush, A. Aminkhani, S. Ershad, G. Karimnezhad, S. Ghammamy, R. Kabiri, Preparation of Zinc (II) and Cadmium (II) Complexes of the Tetradentate Schiff Base Ligand 2-((E)-(2-(2-(pyridine-2-yl)-ethylthio)ethylimino)methyl)-4-bromophenol (PytBrsalH), Molecules 13 (2008) 804–811, https://doi.org/10.3390/molecules13040804.

[4] E.S.A. El-Samanody, S.A. AbouEl-Enein, E.M. Emara, Molecular modeling, spectral investigation and thermal studies of the new asymmetric Schiff base ligand; (E)-N'-(1-(4-((E)-2-hydroxybenzylideneamino)phenyl)ethylidene)morpholine-4-carbothiohydrazide and its metal complexes: evaluation of their antibacterial and anti-molluscicidal activity, Appl. Organomet. Chem. (2018) 32, https://doi.org/10.1002/aoc.4262.

[5] B.L. Vallee, D.S. Auld, Active-site zinc ligands and activated H20 of zinc enzymes (amino acid sequence/metalloenzymes/metalloproteins/structure-function/x-ray crystallography), 1990. doi:10.1073/pnas.87.1.220.

[6] S.F. Sousa, A.B. Lopes, P.A. Fernandes, M.J. Ramos, The Zinc proteome: a tale of stability and functionality, Dalton Trans. (2009) 7946–7956, https://doi.org/10.1039/b904404c.

[7] W.N. Lipscomb, N. Sträter, Recent advances in zinc enzymology, Chem. Rev. 96 (1996) 2375–2433, https://doi.org/10.1021/CR950042J/ASSET/CR950042J.FP.PNG_V03.

[8] B.L. Vallee, D.S. Auld, Zinc: biological functions and coordination motifs, Acc. Chem. Res. 26 (1993) 543–551, https://doi.org/10.1021/AR00034A005/ASSET/AR00034A005.FP.PNG_V03.

[9] X.X. Sun, C.M. Qi, S.L. Ma, H.B. Huang, W. xiang Zhu, Y.C. Liu, Syntheses and structures of two Zn(II) complexes with the pentadentate Schiff-base ligands, Inorg. Chem. Commun. 9 (2006) 911–914, https://doi.org/10.1016/j.inoche.2006.05.018.

[10] M. Bal, G. Ceyhan, B. Avar, M. Köse, A. Kayraldiz, M. Kurtöglu, Synthesis and X-ray powder diffraction, electrochemical, and genotoxic properties of a new azo-Schiff base and its metal complexes, Turk. J. Chem. 38 (2014) 222–241, https://doi.org/10.3906/kim-1306-28.

[11] T. Eren, M. Kose, K. Sayin, V. McKee, M. Kurtoglu, A novel azo-aldehyde and its Ni (II) chelate; Synthesis, characterization, crystal structure and computational studies of 2-hydroxy-5-{(E)-[4-(*propan*-2-*yl*) *phenyl*]diazenyl}benzaldehyde, J. Mol. Struct. 1065–1066 (2014) 191–198, https://doi.org/10.1016/j.molstruc.2014.02.052.

[12] M. Köse, N. Kurtoglu, Ö. Gümüşsu, M. Tutak, V. McKee, D. Karakaş, M. Kurtoglu, Synthesis, characterization and antimicrobial studies of 2-{(E)-[(2-*hydroxy*-5-*methylphenyl*)*imino*]methyl}-4-[(E)-*phenyldiazenyl*]phenol as a novel azo-azomethine dye, J. Mol. Struct. 1053 (2013) 89–99, https://doi.org/10.1016/j.molstruc.2013.09.013.

[13] B. Cabir, B. Avar, M. Gulcan, A. Kayraldiz, M. Kurtoglu, Synthesis, spectroscopic characterization, and genotoxicity of a new group of azo-oxime metal chelates, Turk. J. Chem. 37 (2013) 422–438, https://doi.org/10.3906/kim-1210-57.

[14] A. Gözel, M. Kose, D. Karakaş, H. Atabey, V. McKee, M. Kurtoglu, Spectral, structural and quantum chemical computational and dissociation constant studies of a novel azo-enamine tautomer, J. Mol. Struct. 1074 (2014) 449–456, https://doi.org/10.1016/j.molstruc.2014.06.033.

[15] Ş. Bitmez, K. Sayin, B. Avar, M. Köse, A. Kayraldiz, M. Kurtołlu, Preparation, spectral, X-ray powder diffraction and computational studies and genotoxic properties of new azo-azomethine metal chelates, J. Mol. Struct. 1076 (2014) 213–226, https://doi.org/10.1016/j.molstruc.2014.07.005.

[16] H. Keypour, M. Shayesteh, M. Rezaeivala, K. Sayin, Dinuclear Cu(II) complexes of compartmental Schiff base ligands formed from unsymmetrical tripodal amines of varying arm lengths: crystal structure of $[Cu_2L1](ClO_4)_2$ and theoretical studies, J. Mol. Struct. 1112 (2016) 110–118, https://doi.org/10.1016/j.molstruc.2016.02.004.

[17] K. Sayin, N. Kurtoglu, M. Kose, D. Karakas, M. Kurtoglu, Computational and experimental studies of 2-[(E)-*hydrazinylidenemethyl*]-6-methoxy-4-[(E)-*phenyldiazenyl*]phenol and its tautomers, J. Mol. Struct. 1119 (2016) 413–422, https://doi.org/10.1016/j.molstruc.2016.04.097.

[18] K. Sayin, D. Karakaş, Structural, spectral, NLO and MEP analysis of the $[MgO_2Ti_2(OPri)_6]$, $[MgO_2Ti_2(OPri)_2(acac)_4]$ and $[MgO_2Ti_2(OPri)_2(bzac)_4]$ by DFT method, Spectrochim. Acta A Mol. Biomol. Spectrosc. 144 (2015) 176–182, https://doi.org/10.1016/j.saa.2015.02.086.

[19] K. Sayin, D. Karakaş, The investigation of the solvent effect on coordination of nicotinato ligand with cobalt(II) complex containing tris(2-benzimidazolylmethyl) amine: a computational study, J. Mol. Struct. 1076 (2014) 244–250, https://doi.org/10.1016/j.molstruc.2014.07.078.

[20] A. Podborska, M. Wojnicki, Spectroscopic and theoretical analysis of $Pd^{2+}-Cl^{-}-H_2O$ system, J. Mol. Struct. 1128 (2017) 117–122, https://doi.org/10.1016/j.molstruc.2016.08.039.

[21] K. Lyczko, Tropolone as anionic and neutral ligand in lead(II) and bismuth(III) complexes: synthesis, structure, characterization and computational studies, J. Mol. Struct. 1127 (2017) 549–556, https://doi.org/10.1016/j.molstruc.2016.08.005.

[22] E. Aktan, A.B. Gündüzalp, Ü.Ö. Özmen, Structural, physicochemical characterization, theoretical studies of carboxamides and their Cu(II), Zn(II) complexes having antibacterial activities against E. coli, J. Mol. Struct. 1128 (2017) 775–784, https://doi.org/10.1016/j.molstruc.2016.09.013.

[23] R. Bourzami, L. Ouksel, N. Chafai, Synthesis, spectral analysis, theoretical studies, molecular dynamic simulation and comparison of anticorrosive activity of an ester and an acid a-Hydroxyphosphonates, J. Mol. Struct. 1195 (2019) 839–849, https://doi.org/10.1016/j.molstruc.2019.06.012.

[24] L. Ouksel, S. Chafaa, R. Bourzami, N. Hamdouni, M. Sebais, N. Chafai, Crystal structure, vibrational, spectral investigation, quantum chemical DFT calculations and thermal behavior of Diethyl [hydroxy (phenyl) methyl] phosphonate, J. Mol. Struct. 1144 (2017) 389–395, https://doi.org/10.1016/j.molstruc.2017.05.029.

[25] L. Ouksel, R. Bourzami, S. Chafaa, N. Chafai, Solvent and catalyst-free synthesis, corrosion protection, thermodynamic, MDS and DFT calculation of two environmentally friendly inhibitors: bis-phosphonic acids, J. Mol. Struct. 1222 (2020), 128813, https://doi.org/10.1016/j.molstruc.2020.128813.

[26] L. Ouksel, R. Bourzami, N. Hamdouni, A. Boudjada, Synthesis, supramolecular structure, spectral properties and correlation between nonlinear optic, thermochemistry and thermal behavior of an α-Hydroxyphosphonate acid ester, dual experimental and DFT approaches, J. Mol. Struct. 1229 (2021), 129792, https://doi.org/10.1016/j.molstruc.2020.129792.

[27] H. Tlidjane, N. Chafai, S. Chafaa, C. Bensouici, K. Benbouguerra, New thiophene-derived α-aminophosphonic acids: synthesis under microwave irradiations, antioxidant and antifungal activities, DFT investigations and SARS-CoV-2 main protease inhibition, J. Mol. Struct. 1250 (2022), 131853, https://doi.org/10.1016/j.molstruc.2021.131853.

[28] A. Tabbiche, A. Bouchama, N. Chafai, F. Zaidi, C. Chiter, M. Yahiaoui, A. Abiza, New bis hydrazone: synthesis, X-ray crystal structure, DFT computations, conformational study and in silico study of the inhibition activity of SARS-CoV-2, J. Mol. Struct. 1261 (2022), 132865, https://doi.org/10.1016/j.molstruc.2022.132865.

[29] R. Kerkour, N. Chafai, O. Moumeni, S. Chafaa, Novel α-aminophosphonate derivates synthesis, theoretical calculation, Molecular docking, and in silico prediction of potential inhibition of SARS-CoV-2, J. Mol. Struct. 1272 (2023), 134196, https://doi.org/10.1016/j.molstruc.2022.134196.

[30] R. Satheeshkumar, K. Prabha, K. Natesan Vennila, K. Sayin, E. Güney, W. Kaminsky, R. Acevedo, Spectroscopic (FT-IR, NMR, single crystal XRD) and DFT studies including FMO, Mulliken charges, and Hirshfeld surface analysis, molecular docking and ADME analyses of 2-amino-4′-fluorobenzophenone (FAB), J. Mol. Struct. 1267 (2022), 133552, https://doi.org/10.1016/j.molstruc.2022.133552.

[31] A. Aktaş, W. Nassif, K. Sayin, Investigations of structural, spectral (IR, $^{1}$H-, $^{9}$F-, $^{11}$B-, $^{13}$C-, $^{15}$N-, $^{17}$O-NMR) and anticancer properties of 5FU@B12N12 complexes, Chem. Pap. 75 (2021) 1727–1737, https://doi.org/10.1007/s11696-020-01433-6.

[32] O. Şahin, Ç. Albayrak, M. Odabaşoğlu, O. Büyükgüngör, E)-5-(4-Ethylphenyldiazenyl)salicylaldehyde, Acta Crystallogr. Sect. E Struct. Rep. Online. 61 (2005), https://doi.org/10.1107/S1600536805036834.

[33] Bruker, APEX2 and SAINT. Bruker AXS Inc. (1998).

[34] G.M. Sheldrick, IUCr, A short history of SHELX, Acta Cryst. 64 (2007) 112–122, https://doi.org/10.1107/S0108767307043930.

[35] R. Dennington, T. Keith, J. Millam, GaussView, Version 5.0.8, Semichem Inc., Shawnee Mission KS, 2009 (n.d), http://www.sciepub.com/reference/291346 (accessed December 29, 2022).

[36] M.J. Frisch, G. Trucks, H.B. Schlegel, G.E. Scuseria, M.A. Robb, J. Cheeseman, G. Scalmani, V. Barone, B. Mennucci, G.A. Petersson, H. Nakatsuji, M. Caricato, X. Li, H.P. Hratchian, A.F. Izmaylov, J. Bloino, G. Zheng, J. Sonnenberg, M. Hada, D. Fox, Gaussian 09 Revision A.1, Gaussian Inc, Wallingford CT, 2009.

[37] PerkinElmer ChemBioDraw Ultra Version (13.0.0.3015) CambridgeSoft Waltham, MA, USA, (2012).

[38] Y. Zhao, D.G. Truhlar, The M06 suite of density functionals for main group thermochemistry, thermochemical kinetics, noncovalent interactions, excited states, and transition elements: two new functionals and systematic testing of four M06-class functionals and 12 other functionals, Theor. Chem. Acc. 120 (2008) 215–241, https://doi.org/10.1007/s00214-007-0310-x.

[39] Y. Zhao, D.G. Truhlar, Density functionals with broad applicability in chemistry, Acc. Chem. Res. 41 (2008) 157–167, https://doi.org/10.1021/ar700111a.

[40] Schrödinger, Schrödinger Release 2021-2: epik LLC, New York, NY (2021).

[41] Schrödinger, Schrödinger Release 2021-2: protein Preparation Wizard; Epik, LLC, New York, NY (2021).

[42] Schrödinger, Schrödinger Release 2021-2: siteMap, LLC, New York, NY (2021).

[43] G. Kurtoglu, B. Avar, H. Zengin, M. Kose, K. Sayin, M. Kurtoglu, A novel azo-azomethine based fluorescent dye and its Co(II) and Cu(II) metal chelates, J. Mol. Liq. 200 (2014) 105–114, https://doi.org/10.1016/J.MOLLIQ.2014.10.012.

[44] S. Menati, A. Azadbakht, R. Azadbakht, A. Taeb, A. Kakanejadifard, Synthesis, characterization, and electrochemical study of some novel, azo-containing Schiff bases and their Ni(II) complexes, Dyes Pigments 98 (2013) 499–506, https://doi.org/10.1016/J.DYEPIG.2013.04.009.

[45] B. Li, P.W. Ryan, M. Shanahan, A.G. Ryder, K.J. Leister, Fluorescence excitation–emission matrix (EEM) spectroscopy for rapid identification and quality

evaluation of cell culture media components, Appl. Spectrosc. 65 (11) (2011) 1240–1249, https://doi.org/10.1366/11-06383.

[46] K. AL-Adilee, S. Jaber, Synthesis, characterization and biological activities of some metal complexes derived from azo dye ligand 2-[2'-(5-M*ethyl thiazolyl*)a*zo*]-5-dimethylamino benzoic acid, Asian J. Chem. 30 (2018) 1537–1545, https://doi.org/10.14233/ajchem.2018.21222.

[47] M. Tümer, Polydentate Schiff-base ligands and their Cd(II) and Cu(II) metal complexes: synthesis, characterization, biological activity and electrochemical properties, J. Coord. Chem. 60 (2007) 2051–2065, https://doi.org/10.1080/00958970701236727.